Journal of Alzheimer's Disease xx (2021) x–xx
DOI 10.3233/JAD-201583
IOS Press



# Structural Changes in Thalamic Nuclei Across Prodromal and Clinical Alzheimer's Disease

Adam S. Bernstein[a], Steven Z. Rapcsak[b], Michael Hornberger[c] and Manojkumar Saranathan[a,*], the Alzheimer's Disease Neuroimaging Initiative[1]
[a]*University of Arizona, Department of Medical Imaging, Tuscon, AZ, USA*
[b]*University of Arizona, Department of Neurology, Tuscon, AZ, USA*
[c]*Norwich Medical School, Norwich, UK*

Accepted 17 April 2021
Pre-press 18 May 2021

**Abstract**.
**Background:** Increasing evidence suggests that thalamic nuclei may atrophy in Alzheimer's disease (AD). We hypothesized that there will be significant atrophy of limbic thalamic nuclei associated with declining memory and cognition across the AD continuum.
**Objective:** The objective of this work was to characterize volume differences in thalamic nuclei in subjects with early and late mild cognitive impairment (MCI) as well as AD when compared to healthy control (HC) subjects using a novel MRI-based thalamic segmentation technique (THOMAS).
**Methods:** MPRAGE data from the ADNI database were used in this study ($n = 540$). Healthy control ($n = 125$), early MCI ($n = 212$), late MCI ($n = 114$), and AD subjects ($n = 89$) were selected, and their MRI data were parcellated to determine the volumes of 11 thalamic nuclei for each subject. Volumes across the different clinical subgroups were compared using ANCOVA.
**Results:** There were significant differences in thalamic nuclei volumes between HC, late MCI, and AD subjects. The anteroventral, mediodorsal, pulvinar, medial geniculate, and centromedian nuclei were significantly smaller in subjects with late MCI and AD when compared to HC subjects. Furthermore, the mediodorsal, pulvinar, and medial geniculate nuclei were significantly smaller in early MCI when compared to HC subjects.
**Conclusion:** This work highlights nucleus specific atrophy within the thalamus in subjects with early and late MCI and AD. This is consistent with the hypothesis that memory and cognitive changes in AD are mediated by damage to a large-scale integrated neural network that extends beyond the medial temporal lobes.

Keywords: Alzheimer's disease, Alzheimer's disease neuroimaging initiative, mild cognitive impairment, Papez circuit, thalamic nuclei, thalamus, thalamus optimized multi-atlas segmentation, THOMAS



## INTRODUCTION

Alzheimer's disease (AD), the most prevalent form of dementia afflicting over 5.8 million people in the United States [1], has long been linked to pathological changes seen in the medial temporal lobe, mainly the hippocampus [2, 3]. The hippocampus has a well-characterized role in episodic memory [4], the decline of which is a hallmark of AD. Not surprisingly, neuroimaging studies in AD invariably

[1]Data used in preparation of this article were obtained from the Alzheimer's Disease Neuroimaging Initiative (ADNI) database (http://adni.loni.usc.edu). As such, the investigators within the ADNI contributed to design and implementation of ADNI and/or provided data but did not participate in analysis or writing of this report. A complete listing of ADNI investigators can be found at: http://adni.loni.usc.edu/wp-content/uploads/how_to_apply_ADNI_Acknowledgement_List.pdf

*Correspondence to: Manojkumar Saranathan, PhD, 1501 N. Campbell Ave, P.O. Box 245067, Tucson, AZ 85724, USA. Tel.: +1 507 269 0601; E-mail: manojsar@radiology.arizona.edu.

ISSN 1387-2877/$35.00 

show substantial atrophy of the hippocampus [5–10]. While the hippocampus certainly plays a significant role in the pathogenesis of AD, there is growing evidence that the hippocampus is part of a larger network of brain regions implicated in episodic memory, namely the limbic memory circuit, or the Papez circuit [11]. The limbic memory circuit is a set of cortical and subcortical structures and their interconnections that includes the hippocampus, anterior thalamic nuclei (anteroventral, anterodorsal, anteromedial), the fornix, mammillary bodies, and the posterior cingulate region [11]. Given their established role in episodic memory [12], changes anywhere within this circuit could play a role in the memory loss associated with AD. In addition to the limbic memory circuit, the mediodorsal (MD) nucleus has also been shown to serve an important role in memory in conjunction with the perirhinal cortex [13]. However, despite their established role in memory, the anterior nuclei of the thalamus have received very little attention in AD research. Braak et al. [14] found neurofibrillary tangles and amyloid plaques within the anterior nuclei of the thalamus, with the anterodorsal nucleus being the most affected. These findings were confirmed by Rub et al. [15] who found early neurofibrillary tangles in the laterodorsal and anterodorsal nuclei of the thalamus. Further, Ryan et al. [16] found atrophy in thalamic and caudate volume in presymptomatic familial AD even prior to atrophy in hippocampal volume.

While a handful of imaging studies have reported significant decreases in whole thalamus volumes in mild cognitive impairment (MCI), cognitive aging, and AD [5, 17–19] and another has reported regional changes in shape of the dorsomedial thalamus in AD [20], very few studies have focused on individual thalamic nuclei. This is, in large part, due to technical challenges in successful and accurate parcellation of the thalamic nuclei. Conventional cerebrospinal fluid-nulled (CSFn) Magnetization Prepared Rapid Gradient Echo (MPRAGE), which is $T_1$-weighted, and $T_2$-weighted magnetic resonance imaging (MRI) pulse sequences have poor intra-thalamic nuclear contrast. Most attempts to parcellate the thalamus have been based on diffusion MRI techniques [21–25], but this modality is limited by low spatial resolution and a lack of significant diffusion anisotropy in the largely gray-matter thalamus, resulting in poor delineation of small structures such as anteroventral or geniculate nuclei. Others have used diffusion MRI tractography to identify thalamic nuclei based on cortical connections [26–28]. However, the delineated regions tend to be large, and are not based on inherent tissue differences within the thalamic nuclei. More recently, structural imaging-based techniques for parcellating the thalamus have emerged. In one technique, manual segmentation on a set of histological and *ex vivo* imaging data are combined to create an atlas, which was then used to segment the thalamus *in vivo* data using Bayesian inference [29]. Another technique used a multi-atlas approach to segment the thalamus based on a hierarchical statistical shape model [30]. Recent work by Su et al. [31] has demonstrated that a specialized white-matter-nulled (WMn) MPRAGE sequence produces increased contrast within the thalamus. This was combined with a multi-atlas joint label fusion technique to produce parcellations of the thalamus into distinct nuclei in a technique called **TH**alamus **O**ptimized **M**ulti **A**tlas **S**egmentation (THOMAS).

In the very few studies that have investigated differences in thalamic nuclei in MCI and AD, there have been varied results. Iglesias et al. [29] found that in addition to the whole thalamus, six thalamic nuclei, including the anteroventral nucleus, the mediodorsal nucleus, and medial geniculate nucleus, were significantly smaller in a large cohort of only AD subjects (Alzheimer's Disease Neuroimaging Initiative (ADNI) cohort) when compared to healthy controls. In another study, Low et al. [32] found statistically significant differences in volumes among the anterior, lateral, and posterior clusters of thalamic nuclei between healthy controls and AD subjects. However, they found no differences in the volume of the whole thalamus among healthy controls and subjects with MCI and AD despite using the same technique as Iglesias et al. The major finding of their work is that while there is no difference in absolute volumes of the ventral group of thalamic nuclei among the three groups, the ventral nuclei are significantly smaller within the left thalamus than the right thalamus in subjects with AD (i.e., left-right asymmetry), a phenomenon that has been reported for many other brain regions in AD as well [7, 33–37].

In this work, we use a novel thalamic segmentation technique (THOMAS) to investigate changes in thalamic nuclear volumes in subjects with increasingly severe cognitive impairment from healthy controls to AD. We take advantage of the large ADNI database, which includes high-quality structural MRIs for healthy controls, biomarker confirmed subjects with early and late MCI, and AD to get insights into changes in thalamic nuclear volumes at different stages of the disease. With the increasing evidence

of thalamic involvement in the progression of AD, we expected to find increasing atrophy of the AV and MD nuclei of the thalamus throughout the stages of increasing cognitive impairment up to AD. Specifically, we predicted that atrophy of these select nuclei will correlate with clinical and neuropsychological measures of memory function and cognition.

## METHODS

Data used in preparation of this article were obtained from the ADNI database (http://adni.loni.usc.edu). The ADNI was launched in 2003 as a public-private partnership, led by Principal Investigator Michael W. Weiner, MD. The primary goal of ADNI has been to test whether serial MRI, positron emission tomography, other biological markers, and clinical and neuropsychological assessment can be combined to measure the progression of MCI and early AD. For up-to-date information, see http://www.adni-info.org.

### *Biomarker collection*

Baseline CSF samples were obtained in the morning after an overnight fast and processed as previously described [38]. Briefly, CSF was collected into polypropylene collection tubes or syringes provided to each site, then transferred into polypropylene transfer tubes without any centrifugation step followed by freezing on dry ice within 1 h after collection and shipped overnight to the ADNI Biomarker Core laboratory at the University of Pennsylvania Medical Center on dry ice. Aliquots (0.5 ml) were prepared from these samples after thawing (1 h) at room temperature and gentle mixing. The aliquots were stored in bar code-labeled polypropylene vials at –80°C. $A\beta_{1-42}$, tau, and p-tau were measured using the multiplex xMAP Luminex platform (Luminex Corp, Austin, TX) with Innogenetics (INNO-BIA AlzBio3; Ghent, Belgium; for research use-only reagents) immunoassay kit-based reagents. From the cohort used for this study, 399 subjects (healthy controls (HC) = 72, early MCI (EMCI) = 157, late MCI (LMCI) = 97, AD = 73) had $A\beta_{1-42}$ values available, 488 (HC = 108, EMCI = 195, LMCI = 108, AD = 87) subjects had tau values available, and 487 (HC = 107, EMCI = 195, LMCI = 108, AD = 87) subjects had p-tau values available.

### *Imaging data*

To ensure consistency, the ADNI database was searched for all data from subjects that were imaged at baseline using a 3 Tesla scanner using a CSFn-MPRAGE sequence who were either HC or had a diagnosis of EMCI, LMCI, or AD, which resulted in 650 datasets. Subjects were excluded if they did not have a Montreal Cognitive Assessment (MoCA) score recorded which reduced the total to 587 datasets. Finally, subjects whose image registration or segmentation failed (see next section) were excluded from the study, resulting in a final count of 540 subjects included in this study (119 HC, 208 EMCI, 116 LMCI, 91 AD).

For the purposes of this study, the distinction between early and late MCI was based on the criteria used in the ADNI study. These criteria are defined in the ADNI procedures manual (https://adni.loni.usc.edu/wp-content/uploads/2008/07/adni2-procedures-manual.pdf). Specifically, subjects were classified as EMCI if they had a subjective memory concern reported by themselves, their partner, or a clinician and if they scored 9–11 with 16 or more years of education, 5–9 for 8–15 years of education, or 3–6 for 0–7 years of education on the logical memory II subscale of the Wechsler Memory Scale – Revised, and had a Mini-Mental State Examination (MMSE) score between 24 and 30, and had a Clinical Dementia Rating (CDR) of 0.5 in the memory box, and had cognitive and functional performance sufficiently preserved such that the site physician could not make a diagnosis of AD on the screening visit. The criteria for being classified as LMCI were the same as for EMCI except subjects had to score less than or equal to 8 for 16 or more years of education, less than or equal to 4 for 8–15 years of education, or less than or equal to 2 for 0–7 years of education on the logical memory II subscale of the Wechsler Memory Scale – Revised.

### *Data processing*

Thalamic segmentation was implemented using a modification of the original THOMAS method of Su et al. [31] briefly described below. The eleven delineated nuclei are grouped as follows:

i. **Medial group:** mediodorsal (MD) nucleus, centromedian (CM) nucleus, habenula (Hb).
ii. **Posterior group**: Pulvinar (Pul) nucleus, medial geniculate nucleus (MGN), lateral geniculate nucleus (LGN).
iii. **Lateral group:** Ventral posterolateral (VPL), ventral lateral anterior (VLa) nucleus, ventral lateral posterior (VLp) nucleus, ventral anterior (VA) nucleus.
iv. **Anterior group:** Anteroventral (AV) nucleus.

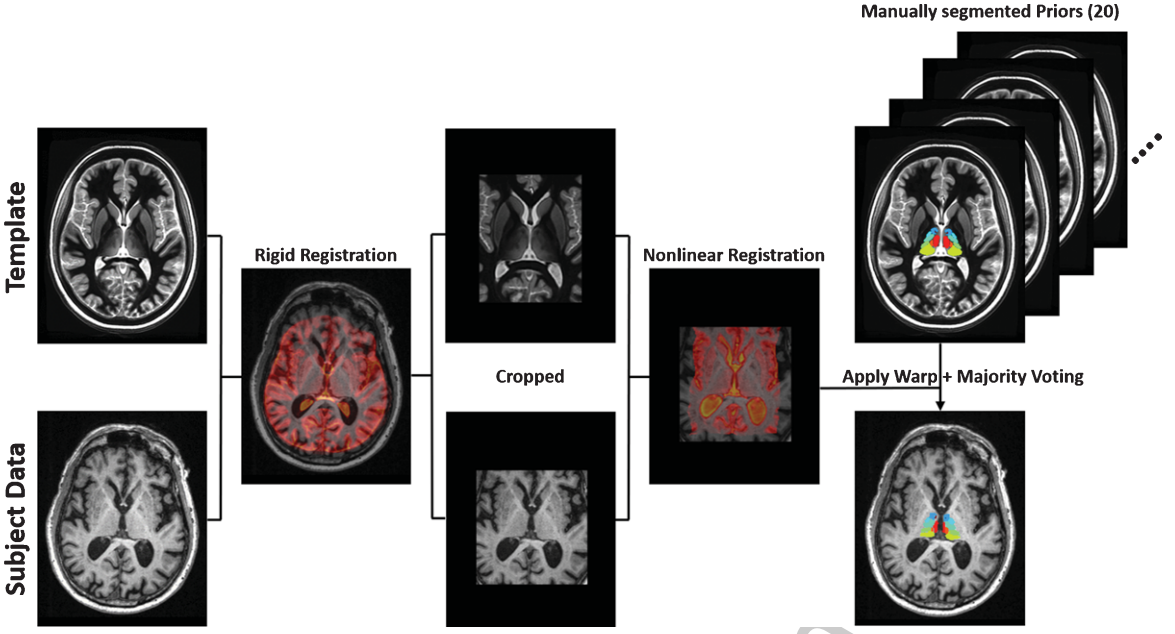


Fig. 1. Multi-atlas segmentation scheme for thalamic nuclei segmentation. The multi-atlas consists of 20 manually segmented WMn MPRAGE datasets, which are warped to subject space and label fused using a majority voting scheme. A WMn template is used as an intermediate step to improve robustness and cropping is performed to improve speed and accuracy.

In 9 healthy control WMn-MPRAGE datasets, eleven thalamic nuclei and the mammillothalamic tract (MTT) were manually segmented by an expert neuroradiologist using the Morel stereotactic atlas as a guide to create a multi atlas. A mean brain template was created from the library of manually segmented datasets (priors). The *buildtemplate* feature of *Advanced Normalization Tools (ANTs)* package [39] was used to iteratively register each prior to an average of the priors and then to create a mean template by averaging the registered priors, which has excellent SNR and image contrast. To segment the thalami of individual subjects, the template image was first registered to the subject's T1-weighted image using the nonlinear symmetric image normalization (SyN) algorithm implemented in *ANTs*. Each anatomical prior was also registered to the template image and these were available *a priori* [39, 40]. A single composite transformation to warp each anatomical prior to each subject's T1-weighted image was then generated by combining the prior to template warp with the template to subject warp. This composite transformation was applied to all thalamic nuclei labels from each of the anatomical priors, to produce 9 sets of thalamic nuclei labels aligned with each subject's image. Finally, the 9 sets of labels were fused into a single set of labels using majority voting as implemented in *ANTs,* producing a single set of thalamic nuclei labels aligned to each individual subject. These steps are shown in Fig. 1. An example T1 MPRAGE image segmented using the modified THOMAS algorithm is shown in three planes in Fig. 2.

These segmented labels were then used to estimate the volume of each thalamic nucleus. In addition to nuclei volumes, a laterality index (LI) was also calculated for all thalamic nuclei as LI = (L-R) / (0.5 * (*L* + R)) * 100% as described by Low et al. [32] In addition to thalamic nuclei volumes, the volumes of bilateral hippocampi were estimated using *FreeSurfer* (version 7.0.0). Intracranial volumes (ICV) were also computed for each subject using *FreeSurfer's recon-all* command.

Note that in the original implementation of THOMAS, joint fusion was used to combine the labels as the input images were white-matter-nulled MP-RAGE images. In order to validate the accuracy of the modified THOMAS method using conventional CSFn-MPRAGE versus WMn-MPRAGE, we performed a comparison on 18 healthy subjects, where both sequences were acquired. The WMn-MPRAGE was segmented using THOMAS with label fusion as described in Su et al. and served as a "gold standard". The CSFn-MPRAGE data was segmented

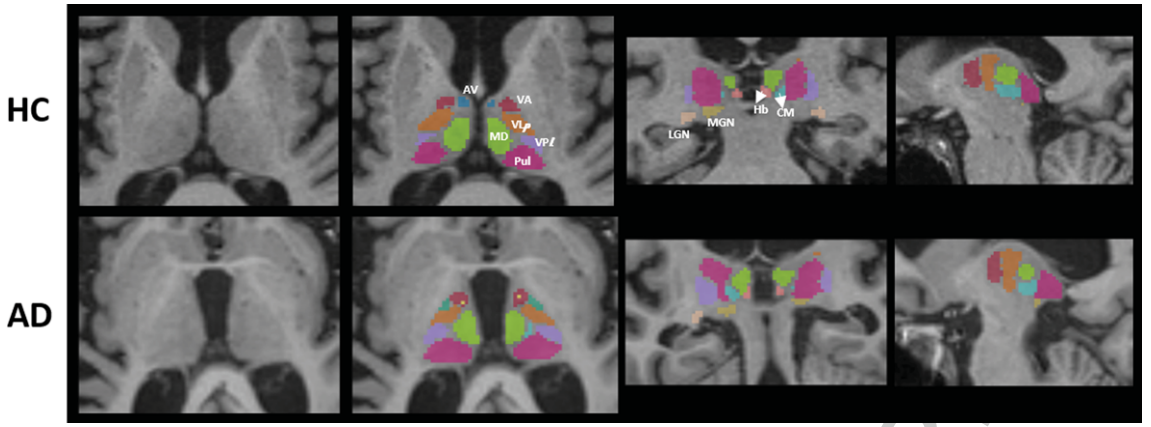


Fig. 2. Thalamic nuclei segmentation labels from the modified THOMAS method overlaid on MPRAGE on a representative healthy control subject (top row) and a representative Alzheimer's disease subject (bottom row).

using THOMAS with majority voting as described above. Accuracy of the proposed majority voting-based THOMAS method was assessed by computing Dice coefficients and a volume similarity index (VSI) between the results obtained from the majority voting method technique compared to those obtained from the WMn-MPRAGE data using joint fusion THOMAS algorithm. Dice coefficients and the volume similarity index (VSI) are calculated as:

$$DICE\ Coefficient = \frac{2\,|X \cap Y|}{|X| + |Y|}\ and$$

$$VSI = 1 - \frac{abs\,(|X| - |Y|)}{|X| + |Y|}$$

where X and Y refer to the two segmentation labels being compared, with one being the ground truth (the WMn MPRAGE results in this case). |X| and |Y| refer to the number of voxels in X and Y respectively.

*Statistical analysis*

All statistical analyses were performed using *XLSTAT* (version 2020.1). Continuous variables were tested for normality (Kolmogorov-Smirnov test). Variables reported as a proportion were analyzed using a chi-square test. The data were independently analyzed for the thalamus and the hippocampus. Age, biological sex, years of education, and ICV were considered as potential covariates for analysis of covariance testing (ANCOVA) and were assessed for potential inclusion in the model. ANCOVA was used to determine if the volumes of each of the thalamic nuclei differed between the four groups of subjects (HC, EMCI, LMCI, AD), followed by pairwise analysis between HC and the remaining three groups with multiple comparison adjustment (Dunnett's test). The least squares estimate of the volumes after adjusting for covariates were obtained, and effects associated with an adjusted $p < 0.05$ were considered statistically significant. Effect sizes for each pair-wise comparison were computed as the Cohen's d score.

Pearson's correlation coefficient (denoted r in this work) of thalamic nuclear volume, in addition to the whole thalamus and hippocampus volumes with neuropsychological test scores, clinical evaluations and biomarker levels were computed to assess the relationship of volume changes to changes in clinical presentation and disease severity. Neuropsychological scores considered were the MoCA, the MMSE, and four measures from the Rey auditory verbal learning test (RAVLT) including the immediate recall (the sum of trials 1–5), the number of words learned (the difference between trial 5 and trial 1), the number of words forgotten (the difference between trial 5 and the delayed recall trial), and the percent of words forgotten. Clinical measures of cognitive function included the CDR and the Alzheimer's disease assessment scale with 13 elements (ADAS13). Finally, the biomarkers included, when available, were Tau protein levels, phosphorylated Tau (Ptau) protein levels, and amyloid-β (Aβ) protein levels.

## RESULTS

*Participant characteristics*

Demographic and clinical characteristics of the included subjects are summarized in Table 1. There was a significant difference in age ($p < 0.001$) across

Table 1
Subject Demographics

| | HC | EMCI | LMCI | AD | *p* |
|---|---|---|---|---|---|
| Number of Subjects | 125 | 212 | 114 | 89 | |
| Sex (% Male) | 45.38% | 51.92% | 47.41% | 53.85% | |
| Age (SD) | 73.42 (6.25) | 70.60 (7.16) | 71.81 (7.93) | 74.06 (7.74) | <0.001 |
| Education (SD) | 16.62 (2.47) | 16.01 (2.69) | 16.61 (2.50) | 16.08 (2.52) | 0.062 |
| MMSE (SD) | 29.10 (1.16) | 28.44 (1.55) | 27.67 (1.81) | 23.01 (2.20) | <0.001 |
| MoCA (SD) | 25.77 (2.43) | 24.04 (2.86) | 22.53 (3.40) | 16.96 (4.67) | <0.001 |
| RAVLT Immediate Recall (SD) | 45.92 (10.59) | 40.65 (10.75) | 34.13 (10.93) | 22.91 (7.83) | <0.001 |
| RAVLT Learned (SD) | 5.90 (2.36) | 5.51 (2.50) | 3.74 (2.63) | 1.80 (1.60) | <0.001 |
| RAVLT Forgotten (SD) | 3.90 (2.77) | 4.39 (2.70) | 4.96 (2.44) | 4.51 (1.65) | 0.042 |
| RAVLT %-Forgotten (SD) | 36.77 (27.88) | 46.84 (30.51) | 66.33 (31.04) | 90.17 (19.52) | <0.001 |
| CDR (SD) | 0.03 (0.14) | 1.31 (0.78) | 1.71 (0.99) | 4.40 (1.78) | <0.001 |
| ADAS13 (SD) | 9.13 (4.42) | 12.23 (5.15) | 17.92 (7.04) | 31.70 (8.54) | <0.001 |
| Aβ (SD) ($n=399$) | 1019.57 (387.10) | 973.47 (358.39) | 817.13 (288.11) | 660.40 (250.41) | <0.001 |
| Tau (SD) ($n=488$) | 238.09 (97.12) | 252.95 (121.05) | 302.34 (132.68) | 380.31 (141.23) | <0.001 |
| PTau (SD) ($n=487$) | 21.99 (9.98) | 23.96 (13.77) | 29.39 (14.49) | 37.63 (15.20) | <0.001 |

MMSE, Mini-Mental State Exam; MoCA, Montreal Cognitive Assessment; RAVLT, Rey Auditory Verbal Learning Test; CDR, Clinical Dementia Rating; ADAS13, Alzheimer's disease assessment scale with 13 elements; Aβ, amyloid-β.

the groups, and a trend toward significance in years of education ($p=0.062$). There were significant differences in all neuropsychological measures including MMSE ($p<0.001$), MoCA ($p<0.001$), RAVLT immediate recall ($p<0.001$), RAVLT number learned ($p<0.001$), RAVLT number forgotten ($p=0.042$), and RAVLT percent forgotten ($p<0.001$). All neuropsychological test scores demonstrated worse performance, on average, with increasing disease severity. Clinical scores were also significantly different, including CDR-SB ($p<0.001$) and ADAS13 ($p<0.001$). Finally, biological CSF markers were also significantly different across groups, including Tau ($p<0.001$) and PTau ($p<0.001$), as well as Aβ ($p<0.001$).

*Assessment of modified THOMAS technique*

Dice coefficients for thalamic nuclei volume estimation compared between the WMn-MPRAGE data used as a gold standard and the CSFn-MPRAGE demonstrated good agreement between both techniques. Dice coefficients ranged from a minimum of 0.67 in the VLa and VPL nuclei to 0.85 for MD and Pulvinar and 0.92 for the whole thalamic volume. Dice coefficients and the VSIs for all nuclei are shown in Supplementary Table 1. It is worth noting that even for small nuclei such as AV and CM, Dice indices of 0.74 and 0.76 were achieved, attesting to the accuracy of the method.

*Comparison of thalamic nuclei volumes*

Initial ANCOVA analysis using age, ICV, biological sex, and years of education revealed that biological sex and years of education did not significantly impact measures of volume for any of the thalamic nuclei nor the hippocampus, and were thus removed from the model. Thus, only age and ICV were included as covariates for this analysis.

The volumes of individual thalamic nuclei, as well as the whole thalamus and the hippocampus for all subjects across all four study groups are shown in Fig. 3. *Post hoc* analysis revealed that in the bilateral MD nuclei, the left Pulvinar nucleus, and the left MGN nucleus, there were significant differences in the volumes between healthy controls and in subjects with EMCI. The volumes of the bilateral AV nuclei, bilateral MD-Pf, the bilateral Pulvinar nuclei, the bilateral CM nuclei, the left MGN nucleus, and the entire thalamus bilaterally were significantly smaller in LMCI subjects when compared to HC subjects. Further, the volumes of the AV nucleus, the Pulvinar nucleus, the MGN, the CM nucleus, and the MD-Pf nucleus in subjects with AD were significantly smaller bilaterally compared to HC subjects. The hippocampus was significantly smaller bilaterally in EMCI, LMCI, and AD subjects when compared to the HC group. The full list of statistical results for the above comparisons are detailed in Supplementary Table 2.

Effect size for each of the above *post-hoc* analyses is plotted in Fig. 4 as the Cohen's d score. The effect size of HC versus EMCI is plotted in blue, the effect size of HC versus LMCI is plotted in orange, and the effect size of HC versus AD is plotted in yellow. On both the left and the right side of the brain, the whole thalamus has a very large effect size ($d=0.70$ on the left, and $d=0.76$ on the right), followed by the

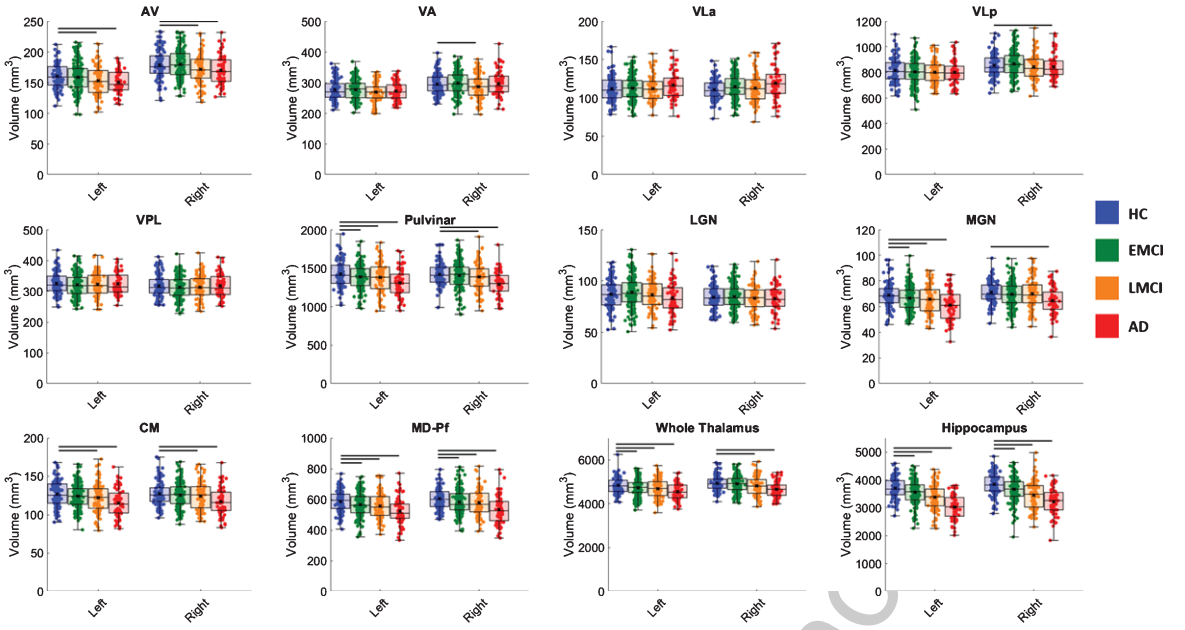


Fig. 3. Thalamic nuclei volumes plotted as box and whisker plots compared across four groups. In the above plots, healthy controls (HC) are plotted in blue, early mild cognitive impairment (EMCI) is plotted in green, late mild cognitive impairment (LMCI) is plotted in orange, and Alzheimer's disease (AD) is plotted in red. Each subject's nuclei volume is plotted as a filled circle on the plot. The black "x" on each box and whisker plot denotes the mean volume for each group. Statistically significant differences ($p < 0.05$) in pairwise comparisons after Dunnett's test are shown as black bars above the box and whisker plots.

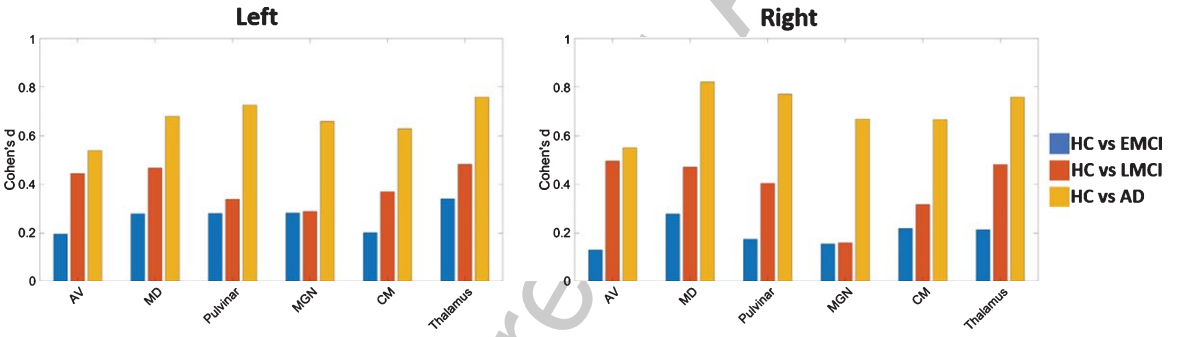


Fig. 4. Effect sizes plotted as Cohen's d computed from pairwise comparisons of healthy controls (HC) with early mild cognitive impairment (EMCI), late mild cognitive impairment (LMCI), and Alzheimer's disease (AD), in the thalamic nuclei shown to have statistically significant differences in volume.

Pulvinar nucleus ($d = 0.68$ on the left and $d = 0.76$ on the right) when comparing HC to AD. As expected, the majority of the nuclei show progressively larger effect sizes with increasing disease severity.

In addition to comparing nuclei volumes, the LI was used to compare asymmetry in the atrophy of nuclei with disease severity. ANCOVA analysis showed no statistically significant differences in the LI (data not shown) for any of the thalamic nuclei. While there was no statistically significant difference in laterality of the nuclei with increasing disease severity, there were several nuclei that were consistently smaller on one side than the other across all disease states. The AV, VA, and MGN nuclei were all generally smaller in the left hemisphere.

### *Correlation of thalamic nuclear volumes to neurocognitive scores*

Pearson correlation coefficients between nuclei that were significantly smaller in the cognitively impaired subjects (EMCI, LMCI, AD) and healthy

Table 2
Pearson's correlation coefficient (β) and associated *p*-values of the anteroventral (AV), mediodorsal (MD-Pf), pulvinar (Pul), medial geniculate nuclei (MGN), centromedian nuclei (CM), and the entire thalamus and hippocampus with select neurocognitive scores, clinical assessments, and biomarker levels

| | MoCA | | RAVLT Immediate | | RAVLT Delayed | | CDR | | ADAS13 | | Tau | | Ptau | | Aβ | |
|---|---|---|---|---|---|---|---|---|---|---|---|---|---|---|---|---|
| | r | *p* | r | *p* | r | *p* | r | *p* | r | *p* | r | *p* | r | *p* | r | *p* |
| AV | 0.198 | <0.001 | 0.173 | <0.001 | 0.138 | 0.002 | –0.217 | <0.001 | –0.228 | <0.001 | –0.168 | <0.001 | –0.158 | <0.001 | 0.079 | 0.117 |
| MD-Pf | 0.273 | <0.001 | 0.246 | <0.001 | 0.157 | <0.001 | –0.199 | <0.001 | –0.268 | <0.001 | –0.034 | 0.459 | –0.036 | 0.427 | 0.103 | 0.040 |
| Pulvinar | 0.262 | <0.001 | 0.241 | <0.001 | 0.156 | <0.001 | –0.176 | <0.001 | –0.276 | <0.001 | –0.089 | 0.048 | –0.091 | 0.045 | 0.169 | <0.001 |
| MGN | 0.229 | <0.001 | 0.171 | <0.001 | 0.130 | 0.003 | –0.176 | <0.001 | –0.247 | <0.001 | –0.010 | 0.830 | –0.014 | 0.756 | 0.098 | 0.051 |
| CM | 0.226 | <0.001 | 0.206 | <0.001 | 0.132 | 0.003 | –0.165 | <0.001 | –0.234 | <0.001 | 0.023 | 0.617 | 0.021 | 0.627 | 0.070 | 0.166 |
| Thalamus | 0.276 | <0.001 | 0.256 | <0.001 | 0.148 | 0.007 | –0.204 | <0.001 | –0.286 | <0.001 | –0.042 | 0.353 | –0.041 | 0.366 | 0.156 | 0.002 |
| Hippocampus | 0.397 | <0.001 | 0.355 | <0.001 | 0.315 | <0.001 | –0.395 | <0.001 | –0.481 | <0.001 | –0.273 | <0.001 | –0.258 | <0.001 | 0.266 | <0.001 |

controls and neurocognitive test scores, clinical scores, and biomarker levels, and their corresponding statistical significance are summarized in Table 2. All nuclei demonstrated statistically significant, albeit weak correlations with MoCA scores, as well as with RAVLT Immediate and delayed recall scores. CDR and ADAS13 were also correlated to thalamic nuclear volumes. The AV nucleus and the Pulvinar nucleus were the only nuclei whose volumes correlated to Tau and P-Tau levels. The MD nucleus and Pulvinar nucleus were the only nuclei to correlate with Aβ levels.

## DISCUSSION

In this study, we investigated changes in the volumes of thalamic nuclei throughout disease progression, i.e., early MCI, late MCI, and finally AD using a novel, accurate thalamic segmentation method. We showed that there are statistically significant differences in several thalamic nuclei at different stages of cognitive impairment, with increasingly smaller volumes with increasing disease severity. Notably, the AV nucleus, a component of the limbic memory circuit, was significantly smaller in subjects with LMCI and AD than in HC subjects. Further, the MD-Pf nucleus, a structure with a well-known role in memory, was also significantly smaller in subjects with EMCI, LMCI, and AD. Additionally, the CM nucleus, which has been shown to have numerous connections within the limbic system [41], was significantly smaller in LMCI and AD than in HC subjects. The findings presented in this work highlight the utility and sensitivity of the thalamic segmentation algorithm and are consistent with other findings suggesting that pathological changes in the thalamus, and more broadly, the limbic memory circuit, play a significant role in the progression of AD.

Notably, the AV nucleus is demonstrably smaller in subjects with increasingly severe cognitive impairment. This result is consistent with the hypothesis that the anterior thalamus plays an important role in the development of the memory impairment that characterizes the early stages of AD [11, 12, 42]. More broadly, Argyropoulos et al. have shown that consideration of structural/functional changes within the entire Papez circuit better explains declining memory performance in subjects with autoimmune limbic encephalitis than hippocampal atrophy alone [42]. The findings presented here and those described elsewhere suggest that a more comprehensive analysis of the entire limbic memory circuit, including the thalamus, the hippocampus, the cingulate gyrus, and their white matter connections may provide more complete insight into the neural substrates of memory loss in AD. Other nuclei from the limbic system, namely the MD-Pf and the CM nuclei showed similar patterns of decreasing volume with disease severity, further promoting the idea that memory loss in AD involves damage to a network of limbic structures and their connections.

In addition to the limbic nuclei discussed above, the pulvinar nucleus and the MGN also showed significant differences in volume with disease severity. In the work by Iglesias et al. [29], they demonstrated a statistically significant difference in the volume of the MGN in subjects with AD. Further, amyloid plaques have been documented throughout the pulvinar nucleus in patients with AD [43]. The pulvinar nucleus has widespread connections throughout the cortex, including visual areas and memory-related regions within the default mode network such as the lateral and medial parietal cortex, as well as the precuneus and parahippocampal gyri. Disruption of these thalamocortical networks may contribute to visual and memory disturbances in AD [44].

Low et al. [32] demonstrated asymmetrical atrophy of the ventral thalamic nuclei in AD, with the left nuclei atrophying significantly more than the right nuclei. In the present work, we were unable to replicate this finding for any thalamic nuclei. There are several plausible explanations for this discrepancy. In their work, there are relatively few subjects ($n = 65$) relative to what was used here ($n = 540$) from the ADNI study, making their analysis more susceptible to Type II errors. Further, they utilized a different thalamic segmentation software implemented in *FreeSurfer* [29] which was demonstrated to be less reliable (as quantified by poorer dice coefficients using manual segmentation as gold standard) than THOMAS [31]. Other studies have found similar patterns of asymmetrical atrophy for other structures in the brain [37, 45–47], however, so further investigation into the findings by Low are certainly warranted.

While this study took advantage of the large database provided by ADNI, there are a number of limitations that need to be addressed in future investigations. The template and multi-atlas used in this study were based on white-matter nulled T1 images due to the increased contrast of thalamic nuclei using that imaging modality. However, this is not a conventional MRI sequence, and there is limited data available to perform the above analysis. Despite the differing contrast between white-matter nulled and CSF-nulled $T_1$-weighted images, good to excellent reliability of the registration and volume estimation has been demonstrated here (see Supplementary Material) [47, 48]. While this work included healthy controls, EMCI, LMCI, and AD subjects, there was no analysis of thalamic nuclei volumes as HC subjects progress to AD over time, which would arguably provide even more useful data with respect the progression of the disease. Not all subjects included in this analysis with EMCI will progress to LMCI and AD, and thus may show a different pattern of atrophy than subjects with presymptomatic AD. There were simply not enough imaging studies collected at 3T to perform this type of analysis using the ADNI dataset. Further, the distinction between EMCI and LMCI defined in the ADNI, which distinguishes the two based on a single memory test, has been shown to have relatively high false-positive rates [49], an issue that must be addressed in the future if the progression to AD is to be more accurately followed. If the hypothesis that AD is a result of disease throughout the limbic memory circuit, and not just the medial temporal lobe is true, then we would expect to see changes in the white matter pathways that connect the gray matter structures within this circuit. In future work, it will be worthwhile to include white matter metrics, such as those derived from diffusion MRI experiments, to further characterize network-level changes occurring with disease progression.

Many of the above shortcomings of the present study provide exciting opportunities for future work to explore the role of the thalamus, and more broadly, the entire limbic memory circuit in AD. As the field of connectomics is rapidly expanding and improving, rapid and reliable segmentation of the thalamus will provide invaluable information necessary for better understanding thalamic connections to cortical and subcortical regions of the brain. We believe that mapping the entire limbic memory circuit using a multimodal approach including diffusion MRI, functional MRI and structural MRI, will provide a much more comprehensive insight into the neural basis of cognitive changes in AD.

In conclusion, this work highlights the importance of considering individual thalamic nuclei in the progression of AD. The thalamus is a complex structure with widespread connections throughout the brain, and one might expect different thalamic nuclei to be affected differently than others as AD progresses. With recent advances in thalamic parcellation algorithms, we can provide higher degrees of sensitivity and specificity to changes within the thalamus, and provide more insight into the progression of AD. While the hippocampus and other parts of the medial temporal lobe are clearly the most strongly affected regions of the brain in AD, the data provided in this work supports the hypothesis that the episodic memory loss that characterize the early stages of the disease may be mediated, at least in part, by the anterior thalamic components of the Papez circuit and the MD nucleus.

## ACKNOWLEDGMENTS

Data collection and sharing for this project was funded by the Alzheimer's Disease Neuroimaging Initiative (ADNI) (National Institutes of Health Grant U01 AG024904) and DOD ADNI (Department of Defense award number W81XWH-12-2-0012). ADNI is funded by the National Institute on Aging, the National Institute of Biomedical Imaging and Bioengineering, and through generous contributions from the following: AbbVie, Alzheimer's Association; Alzheimer's Drug Discovery Foundation; Araclon Biotech; BioClinica, Inc.; Biogen;

Bristol-Myers Squibb Company; CereSpir, Inc.; Cogstate; Eisai Inc.; Elan Pharmaceuticals, Inc.; Eli Lilly and Company; EuroImmun; F. Hoffmann-La Roche Ltd and its affiliated company Genentech, Inc.; Fujirebio; GE Healthcare; IXICO Ltd.; Janssen Alzheimer Immunotherapy Research & Development, LLC.; Johnson & Johnson Pharmaceutical Research & Development LLC.; Lumosity; Lundbeck; Merck & Co., Inc.; Meso Scale Diagnostics, LLC.; NeuroRx Research; Neurotrack Technologies; Novartis Pharmaceuticals Corporation; Pfizer Inc.; Piramal Imaging; Servier; Takeda Pharmaceutical Company; and Transition Therapeutics. The Canadian Institutes of Health Research is providing funds to support ADNI clinical sites in Canada. Private sector contributions are facilitated by the Foundation for the National Institutes of Health (http://www.fnih.org). The grantee organization is the Northern California Institute for Research and Education, and the study is coordinated by the Alzheimer's Therapeutic Research Institute at the University of Southern California. ADNI data are disseminated by the Laboratory for Neuro Imaging at the University of Southern California.

We also acknowledge the Arizona Alzheimer's Consortium for seed funding to enable data collection and analysis.

Authors' disclosures available online (https://www.j-alz.com/manuscript-disclosures/20-1583r1).

## SUPPLEMENTARY MATERIAL

The supplementary material is available in the electronic version of this article: https://dx.doi.org/10.3233/JAD-201583.

## REFERENCES

[1] (2020) 2020 Alzheimer's disease facts and figures. *Alzheimers Dement* **16**, 391-460.

[2] Setti SE, Hunsberger HC, Reed MN (2017) Alterations in hippocampal activity and Alzheimer's disease. *Transl Issues Psychol Sci* **3**, 348-356.

[3] Craig LA, Hong NS, McDonald RJ (2011) Revisiting the cholinergic hypothesis in the development of Alzheimer's disease. *Neurosci Biobehav Rev* **35**, 1397-1409.

[4] Squire LR, Stark CEL, Clark RE (2004) The medial temporal lobe. *Annu Rev Neurosci* **27**, 279-306.

[5] Roh JH, Qiu A, Seo SW, Soon HW, Kim JH, Kim GH, Kim MJ, Lee JM, Na DL (2011) Volume reduction in subcortical regions according to severity of Alzheimer's disease. *J Neurol* **258**, 1013-1020.

[6] Bobinski M, De Leon MJ, Wegiel J, Desanti S, Convit A, Saint Louis LA, Rusinek H, Wisniewski HM (1999) The histological validation of post mortem magnetic resonance imaging- determined hippocampal volume in Alzheimer's disease. *Neuroscience* **95**, 721-725.

[7] Shi F, Liu B, Zhou Y, Yu C, Jiang T (2009) Hippocampal volume and asymmetry in mild cognitive impairment and Alzheimer's disease: Meta-analyses of MRI studies. *Hippocampus* **19**, 1055-1064.

[8] Aschenbrenner AJ, Gordon BA, Benzinger TLS, Morris JC, Hassenstab JJ (2018) Influence of tau PET, amyloid PET, and hippocampal volume on cognition in Alzheimer disease. *Neurology* **91**, e859-e866.

[9] Thaker AA, Weinberg BD, Dillon WP, Hess CP, Cabral HJ, Fleischman DA, Leurgans SE, Bennett DA, Hyman BT, Albert MS, Killiany RJ, Fischl B, Dale AM, Desikan RS (2017) Entorhinal cortex: Antemortem cortical thickness and postmortem neurofibrillary tangles and amyloid pathology. *Am J Neuroradiol* **38**, 961-965.

[10] Kulason S, Tward DJ, Brown T, Sicat CS, Liu CF, Ratnanather JT, Younes L, Bakker A, Gallagher M, Albert M, Miller MI (2019) Cortical thickness atrophy in the transentorhinal cortex in mild cognitive impairment. *Neuroimage Clin* **21**, 101617.

[11] Aggleton JP (2012) Multiple anatomical systems embedded within the primate medial temporal lobe: Implications for hippocampal function. *Neurosci Biobehav Rev* **36**, 1579-1596.

[12] Aggleton JP, Pralus A, Nelson AJD, Hornberger M (2016) Thalamic pathology and memory loss in early Alzheimer's disease: Moving the focus from the medial temporal lobe to Papez circuit. *Brain* **139**(Pt 7), 1877-1890.

[13] Aggleton JP, Brown MW (1999) Episodic memory, amnesia, and the hippocampal-anterior thalamic axis. *Behav Brain Sci* **22**, 425-444.

[14] Braak H, Braak E (1991) Alzheimer's disease affects limbic nuclei of the thalamus. *Acta Neuropathol* **81**, 261-268.

[15] Rüb U, Stratmann K, Heinsen H, Del Turco D, Ghebremedhin E, Seidel K, Den Dunnen W, Korf HW (2015) Hierarchical distribution of the tau cytoskeletal pathology in the thalamus of Alzheimer's disease patients. *J Alzheimers Dis* **49**, 905-915.

[16] Ryan NS, Keihaninejad S, Shakespeare TJ, Lehmann M, Crutch SJ, Malone IB, Thornton JS, Mancini L, Hyare H, Yousry T, Ridgway GR, Zhang H, Modat M, Alexander DC, Rossor MN, Ourselin S, Fox NC (2013) Magnetic resonance imaging evidence for presymptomatic change in thalamus and caudate in familial Alzheimer's disease. *Brain* **136**(Pt 5), 1399-1414.

[17] De Jong LW, Van Der Hiele K, Veer IM, Houwing JJ, Westendorp RGJ, Bollen ELEM, De Bruin PW, Middelkoop HAM, Van Buchem MA, Van Der Grond J (2008) Strongly reduced volumes of putamen and thalamus in Alzheimer's disease: An MRI study. *Brain* **131**(Pt 12), 3277-3285.

[18] Pini L, Pievani M, Bocchetta M, Altomare D, Bosco P, Cavedo E, Galluzzi S, Marizzoni M, Frisoni GB (2016) Brain atrophy in Alzheimer's disease and aging. *Ageing Res Rev* **30**, 25-48.

[19] Watson R, Colloby SJ, Blamire AM, O'Brien JT (2016) Subcortical volume changes in dementia with Lewy bodies and Alzheimer's disease. A comparison with healthy aging. *Int Psychogeriatrics* **28**, 529-536.

[20] Zarei M, Patenaude B, Damoiseaux J, Morgese C, Smith S, Matthews PM, Barkhof F, Rombouts S, Sanz-Arigita E, Jenkinson M (2010) Combining shape and connectivity analysis: An MRI study of thalamic degeneration in Alzheimer's disease. *Neuroimage* **49**, 1-8.

[21] Battistella G, Najdenovska E, Maeder P, Ghazaleh N, Daducci A, Thiran JP, Jacquemont S, Tuleasca C, Levivier M, Bach Cuadra M, Fornari E (2017) Robust thalamic nuclei segmentation method based on local diffusion magnetic resonance properties. *Brain Struct Funct* **222**, 2203-2216.

[22] Kumar V, Mang S, Grodd W (2015) Direct diffusion-based parcellation of the human thalamus. *Brain Struct Funct* **220**, 1619-1635.

[23] Mang SC, Busza A, Reiterer S, Grodd W, Klose and U (2012) Thalamus segmentation based on the local diffusion direction: A group study. *Magn Reson Med* **67**, 118-126.

[24] Wiegell MR, Tuch DS, Larsson HBW, Wedeen VJ (2003) Automatic segmentation of thalamic nuclei from diffusion tensor magnetic resonance imaging. *Neuroimage* **19**, 391-401.

[25] Ziyan U, Tuch D, Westin CF (2006) Segmentation of thalamic nuclei from DTI using spectral clustering. In *Lecture Notes in Computer Science (including subseries Lecture Notes in Artificial Intelligence and Lecture Notes in Bioinformatics)*. Springer Verlag, pp. 807-814.

[26] Schlaier J, Anthofer J, Steib K, Fellner C, Rothenfusser E, Brawanski A, Lange M (2015) Deep brain stimulation for essential tremor: Targeting the dentato-rubro-thalamic tract? *Neuromodulation Technol Neural Interface* **18**, 105-112.

[27] Sedrak M, Gorgulho A, Frew A, Behnke E, DeSalles A, Pouratian N (2011) Diffusion tensor imaging and colored fractional anisotropy mapping of the ventralis intermedius nucleus of the thalamus. *Neurosurgery* **69**, 1124-1130.

[28] Yamada K, Akazawa K, Yuen S, Goto M, Matsushima S, Takahata A, Nakagawa M, Mineura K, Nishimura T (2010) MR imaging of ventral thalamic nuclei. *Am J Neuroradiol* **31**, 732-735.

[29] Iglesias JE, Insausti R, Lerma-Usabiaga G, Bocchetta M, Van Leemput K, Greve DN, van der Kouwe A, Fischl B, Caballero-Gaudes C, Paz-Alonso PM (2018) A probabilistic atlas of the human thalamic nuclei combining *ex vivo* MRI and histology. *Neuroimage* **183**, 314-326.

[30] Liu Y, D'Haese PF, Newton AT, Dawant BM (2020) Generation of human thalamus atlases from 7 T data and application to intrathalamic nuclei segmentation in clinical 3 T T1-weighted images. *Magn Reson Imaging* **65**, 114-128.

[31] Su JH, Thomas FT, Kasoff WS, Tourdias T, Choi EY, Rutt BK, Saranathan M (2019) Thalamus Optimized Multi Atlas Segmentation (THOMAS): Fast, fully automated segmentation of thalamic nuclei from structural MRI. *Neuroimage* **194**, 272-282.

[32] Low A, Mak E, Malpetti M, Chouliaras L, Nicastro N, Su L, Holland N, Rittman T, Rodríguez PV, Passamonti L, Bevan-Jones WR, Jones PS, Rowe JB, O'Brien JT (2019) Asymmetrical atrophy of thalamic subnuclei in Alzheimer's disease and amyloid-positive mild cognitive impairment is associated with key clinical features. *Alzheimers Dement (Amst)* **11**, 690-699.

[33] Wessa M, King A V., Meyer P, Frölich L, Flor H, Poupon C, Hoppstädter M, Linke J (2016) Impaired and preserved aspects of feedback learning in aMCI: Contributions of structural connectivity. *Brain Struct Funct* **221**, 2831-2846.

[34] Yang C, Zhong S, Zhou X, Wei L, Wang L, Nie S (2017) The abnormality of topological asymmetry between hemispheric brain white matter networks in Alzheimer's disease and mild cognitive impairment. *Front Aging Neurosci* **9**, 261.

[35] Thompson PM, Hayashi KM, De Zubicaray G, Janke AL, Rose SE, Semple J, Herman D, Hong MS, Dittmer SS, Doddrell DM, Toga AW (2003) Dynamics of gray matter loss in Alzheimer's disease. *J Neurosci* **23**, 994-1005.

[36] Woolard AA, Heckers S (2012) Anatomical and functional correlates of human hippocampal volume asymmetry. *Psychiatry Res Neuroimaging* **201**, 48-53.

[37] Tetzloff KA, Graff-Radford J, Martin PR, Tosakulwong N, Machulda MM, Duffy JR, Clark HM, Senjem ML, Schwarz CG, Spychalla AJ, Drubach DA, Jack CR, Lowe VJ, Josephs KA, Whitwell JL (2018) Regional distribution, asymmetry, and clinical correlates of tau uptake on [18F]AV-1451 PET in atypical Alzheimer's disease. *J Alzheimers Dis* **62**, 1713-1724.

[38] Shaw LM, Vanderstichele H, Knapik-Czajka M, Clark CM, Aisen PS, Petersen RC, Blennow K, Soares H, Simon A, Lewczuk P, Dean R, Siemers E, Potter W, Lee VMY, Trojanowski JQ (2009) Cerebrospinal fluid biomarker signature in Alzheimer's disease neuroimaging initiative subjects. *Ann Neurol* **65**, 403-413.

[39] Avants BB, Tustison NJ, Stauffer M, Song G, Wu B, Gee JC (2014) The Insight ToolKit image registration framework. *Front Neuroinform* **8**, 44.

[40] Avants BB, Epstein CL, Grossman M, Gee JC (2008) Symmetric diffeomorphic image registration with cross-correlation: Evaluating automated labeling of elderly and neurodegenerative brain. *Med Image Anal* **12**, 26-41.

[41] Vertes RP, Linley SB, Hoover WB (2015) Limbic circuitry of the midline thalamus. *Neurosci Biobehav Rev* **54**, 89-107.

[42] Argyropoulos GPD, Loane C, Roca-Fernandez A, Lage-Martinez C, Gurau O, Irani SR, Butler CR (2019) Network-wide abnormalities explain memory variability in hippocampal amnesia. *Elife* **8**, e46156.

[43] Kuljis RO (1994) Lesions in the pulvinar in patients with Alzheimer's disease. *J Neuropathol Exp Neurol* **53**, 202-211.

[44] Mendez MF, Mendez MA, Martin R, Smyth KA, Whitehouse PJ (1990) Complex visual disturbances in Alzheimer's disease. *Neurology* **40**, 439-443.

[45] Pennanen C, Testa C, Laakso MP, Hallikainen M, Helkala EL, Hänninen T, Kivipelto M, Könönen M, Nissinen A, Tervo S, Vanhanen M, Vanninen R, Frisoni GB, Soininen H, Tuomainen S (2005) A voxel based morphometry study on mild cognitive impairment. *J Neurol Neurosurg Psychiatry* **76**, 11-14.

[46] Wachinger C, Salat DH, Weiner M, Reuter M (2016) Whole-brain analysis reveals increased neuroanatomical asymmetries in dementia for hippocampus and amygdala. *Brain* **139**, 3253-3266.

[47] Kim JH, Lee JW, Kim GH, Roh JH, Kim MJ, Seo SW, Kim ST, Jeon S, Lee JM, Heilman KM, Na DL (2012) Cortical asymmetries in normal, mild cognitive impairment, and Alzheimer's disease. *Neurobiol Aging* **33**, 1959-1966.

[48] Saranathan M, Iglehart C, Monti M, Tourdias T, Rutt BK (2020) *In vivo* structural MRI-based atlas of human thalamic nuclei. *medRxiv*, 2020.08.09.20171314.

[49] Edmonds EC, McDonald CR, Marshall A, Thomas KR, Eppig J, Weigand AJ, Delano-Wood L, Galasko DR, Salmon DP, Bondi MW (2019) Early versus late MCI: Improved MCI staging using a neuropsychological approach. *Alzheimers Dement* **15**, 699-708.